A Confident Configuration for an Environmental Radiation Monitoring System

Dinh Tien Hung, Cao Van Hiep, Pham Dinh Khang, Nguyen Xuan Hai, Nguyen Ngoc Anh, Duc-Tan Tran, Dinh Kim Chien, Nguyen Nhi Dien, and Tien-Anh Nguyen

***Abstract*— This work presents a high-resolution, high-confidence, and high-temperature-stabilization prototype environmental radiation monitoring system (ERMS) with integrated digital filter, peak-finding algorithms, and real-time analyses. Through measuring ^{137}Cs and ^{60}Co radiation sources with the same NaI(Tl) detector, the features of the digital multi-channel analyzer (DMCA) in our system, including throughput, energy resolution, and peak shape, were compared with those of a commercial instrument, namely, the DSPEC jr 2.0 from ORTEC, USA. The results indicate that the FWHM and peak heights obtained with our DMCA are better than those obtained with the DSPEC jr 2.0 up to 12%. The ERMS also integrates a solar power supply, multimodal data transmission, and a weather channel, thus facilitating its deployment in boundary areas or far islands for monitoring and forecasting radioactive propagation. Therefore, the proposed configuration system is highly promising in terms of performance and low cost of maintenance.**

***Index Terms*— Environmental radiation monitoring system, early warning algorithm, digital multi-channel analyzer, temperature stabilization, ambient gamma dose rate.**

I. Introduction

ENVIRONMENTAL radiation monitoring systems (ERMSs) play an important role in monitoring radiation exposure and estimating radioactive propagation induced by nuclear activities or nuclear accidents. Numerous ERMS configurations have been developed worldwide [1]–[6]. For instance, exposure rate conversion circuits, coupled with NaI(Tl) scintillation detectors, have been used for monitoring the radiation fields in light water reactors. Using digital subscriber line and cellular Internet Protocol technologies, a real-time network of portable ERMSs was developed in [2], [3]. However, these systems have not been able to provide quantitative and qualitative information on radiation fields, which is essential for monitoring high-level radiation exposure. After the Fukushima Daiichi nuclear power plant accident, Yang Ishigaki et al. proposed mobile radiation monitoring systems consisting of p-i-n photodiode detectors, which can be connected to smartphones using microphone cables [4]. The combination of the p-i-n photodiode detectors and smartphones helped reduce the production and operation costs. Unfortunately, the proposed system entails A/D conversion, filtering, and a threshold comparison performed by an app installed on the smartphone; thus, its successful operation depends strongly on the smartphone model and generation. Currently, several ERMSs have been granted patents [5]–[7]. However, these commercial ERMSs are expensive, with considerable expenditures going towards repairs and maintenance.

In recent years, technological developments have led to great improvements in the field of ERMSs. Among modern techniques, field programmable gate arrays (FPGAs) and digital signal processing (DSP) have been applied widely in the development of radioactive monitoring equipment [8], [9]. These techniques allow measurement devices to be designed that are low cost, compact, and practical. However, some monitoring stations have not yet integrated meteorological or oceanographic sensors into their measuring systems [3], [4], even though those parameters play an important role in analyzing, simulating, and predicting radioactive dispersion. Furthermore, false alarms, which pose an important problem in the monitoring of radiation exposure, have rarely been mentioned in the literature.

In this study, a low-cost (i.e., with respect to production and maintenance) and confidently configured ERMS was developed. The station's hardware includes three channels for radioactive measurements and one channel for monitoring weather parameters. The system utilizes both FPGA-based DSP and microcontroller techniques to process the signals obtained from its detectors and sensors. Moreover, this configuration features advanced properties, including real-time analyses, a high count rate response, a confident high-dose-level alert mechanism, an embedded algorithms allow the automatic identification of the radio-isotopes, and the combination of exposure rate with meteorological parameters for nuclear

Manuscript received 12 January 2020; revised 5 June 2020; This work is supported by the MICEE Research Project, under Grant No. 634/2017/HDKHCN. Nguyen Xuan Hai and Pham Dinh Khang acknowledge support by the National Foundation for Science and Technology Development (NAFOSTED) of Vietnam through Grant No. 103.04-2019.388.

Dinh Tien Hung, Cao Van Hiep and Dinh Kim Chien are with the Military Institute of Chemical and Environmental Engineering (MICEE), Hanoi 100000, Vietnam (e-mail: dinhtienhungnbc@gmail.com)

Pham Dinh Khang is with Hanoi University of Science and Technology, Hanoi 100000, Vietnam

Nguyen Xuan Hai and Nguyen Nhi Dien are with the Dalat Nuclear Research Institute, Dalat 670000, Vietnam

Nguyen Ngoc Anh is with the Institute of Research and Development, Duy Tan University, Da Nang 550000, Vietnam

Duc-Tan Tran is with the Faculty of Electrical and Electronic Engineering, Phenikaa University, Hanoi 12116, Vietnam

Tien-Anh Nguyen is with the Department of Physics, Le Quy Don Technical University, Hanoi 11917, Vietnam (e-mail: anhnt007@gmail.com)

accident analyses. A prototype was built and installed to test the proposed configuration.

II. Design of the ERMS

A. Hardware Design

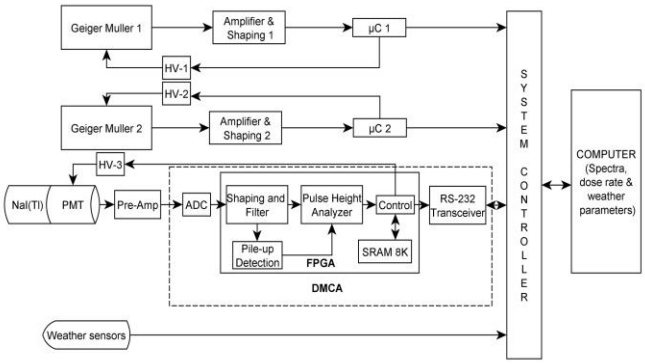

Fig. 1. The design configuration of the ERMS

The basic ERMS design configuration is presented in Fig. 1. The system includes three channels for radioactive measurements and one channel for weather observations. The weather channel consists of sensors for measuring humidity, temperature, wind speed and direction, and rainfall. The radioactivity measurement channels consist of a low-dose-level monitor, a high-dose-level monitor, and a spectrometer. All measured data are transferred to a server via one of four different networks, namely, a cellular, satellite, ethernet, or radio frequency (RF) network. The power is supplied alternately by three sources: a solar panel, a rechargeable battery, and an electrical grid.

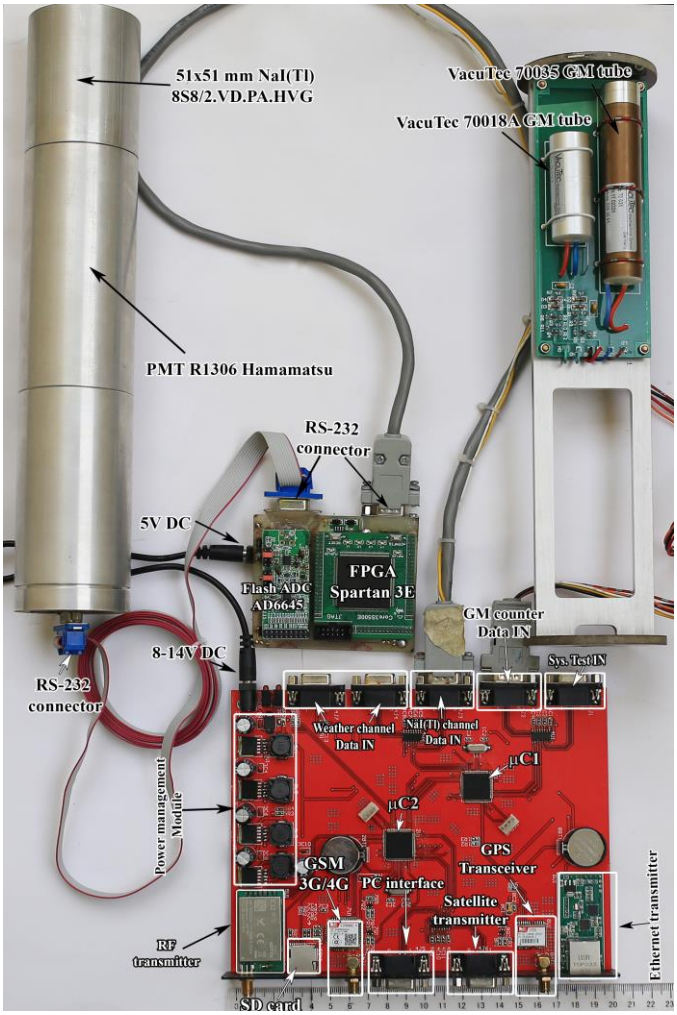

Fig. 2. Photograph of the basic hardware used in the ERMS

The basic hardware components of the ERMS are shown in Fig. 2. The low-gamma-dose-rate monitoring channel (from background level to 1 mSv/h) contains a VacuTec model 70035 Geiger Muller (GM) counter [10], an amplifier-shaper module, a high voltage (HV) power supply, and an AVR ATmega128 low-power 8-bit microcontroller (µC). The pulses output by the GM counter are fed to the amplifier and shaper stage before being digitized by an ADC embedded in the µC. The µC processes these digital data to compute the ambient radiation dose rates. The high-gamma-dose-rate monitoring channel (from 1 mSv/h to 10 Sv/h) has a similar design, but its conversion factor (relating count rates to exposure rates) is different. In this channel, the GM counter is a VacuTec model 70018A counter [11]. The operating voltages of both GM counters are set to 500 V. The switching threshold between the two GM detectors is chosen to be 1 mSv/h after considering the gamma sensitivities of these detectors.

The spectrometer channel consists of a 51×51 mm NaI(Tl) detector (type: 8S8/2.VD.PA.HVG, ScintiTech, USA) coupled to a photomultiplier tube (R1306, Hamamatsu). It can measure gamma rays in the range from 50 keV to 3 MeV. This detector is connected to a low-noise charge-sensitive pre-amplifier. The key component of the spectrometer channel is a digital multi-channel analyzer, which is composed of a 14-bit ADC (Analog Devices AD6645), an FPGA (Xilinx Spartan-3E XC3S500E) with 360 Kbits of fast block RAM, and an RS-232 Transceiver MAX232ESE. The main modules of the digital multichannel analyzer (DMCA) are implemented on the FPGA (Fig. 1). The signals from the preamplifier are amplified by a pre-filter circuit [12] and then digitalized by the ADC AD6645, with the data acquired at a rate of 50 MSPS. In order to optimize functions of modules in the FPGA, the raw data collected from the ADC are used to monitor the performance of the DMCA and improve the reliability of various modules, such as the pulse-shaping filter, threshold discriminator, pile-up detector, and pulse-height analyzer. In the simulation process performed by MATLAB/Simulink, a low-pass filter using Hamming window with a 1.5 MHz cutoff frequency is employed to remove high-frequency harmonics from the ADC [13], [14]. Furthermore, the capacitor resistor filter approach is utilized to filter and shorten the pulse [15]. As a result, the signal-to-noise ratio increases, the baseline drifts are at a minimum, and the pile-up decreases. If the amplitude of the shaped and filtered pulse is higher than a given threshold, a trigger signal is issued to initiate the operation of several other functional blocks: the differentiator, the peak counter, the pile-up detector, and the pulse height analyzer. The differentiator block detects the peak and the pile-up [16], while the counter block counts the number of peaks in the pulse when the signal exceeds the given threshold. All spectrum data formed by peak signals are stored in an 8K SRAM and are transferred externally through an RS-

232 transceiver. Finally, the spectral distortion due to temperature variation is treated via a control program. The control block is responsible for controlling the data acquisition, analysis, storage, and transmission processes. At high ambient dose rates (exceeding 50 μSv/h for 10 seconds), the photomultiplier in the spectrometer will begin to saturate, and the high voltage power supply for the photomultiplier will be switched off automatically by the control block. At which point, the ERMS is operating the GM counter channels simply to prevent damage to the photomultiplier.

The weather channel includes an AIO 2 [17] sonic weather sensor with two-dimensional sonic technology. This technology provides reference-grade accuracy without the need for moving parts. The device includes a built-in compass for the automatic magnetic north alignment of the wind sensor. The sensor is connected directly to the system controller.

The system controller is a combination of two ARM STM32F103VCT6 (ARM Cortex M3) microcontrollers. The first μC receives the measured data from detectors, sensors, and the Global Positioning System (IC SIM28 GPS). Encrypted data transmission from the first μC to server through any of the four different communication mechanisms is controlled by the the second μC. In normal operation mode, the power consumption of the entire system is approximately 5 W (except when using RF transmission). Furthermore, the system controller also carries out the electrical power management function in the ERMS. The dimension and mass of the central box are 200 mm × 200 mm × 15 mm and 200 g, respectively.

B. Software Design and Calculation

The control program for the ERMS was written in the C# programing language. Fig. 3 illustrates the flow of the control algorithm. Under normal conditions, the data transmission interval is 5 minutes for spectrometer data, and 2 minutes for weather parameters and ambient dose rate data. When the gamma radiation dose rate level exceeds the pre-set threshold value, the transmission intervals is reduced to 2 minutes and 1 minute, respectively. To ensure stability for data transfer, the communication module uses abundant transmission methods (cellular network, ethernet, satellite, and RF). Normally, only one method is activated to reduce power consumption.

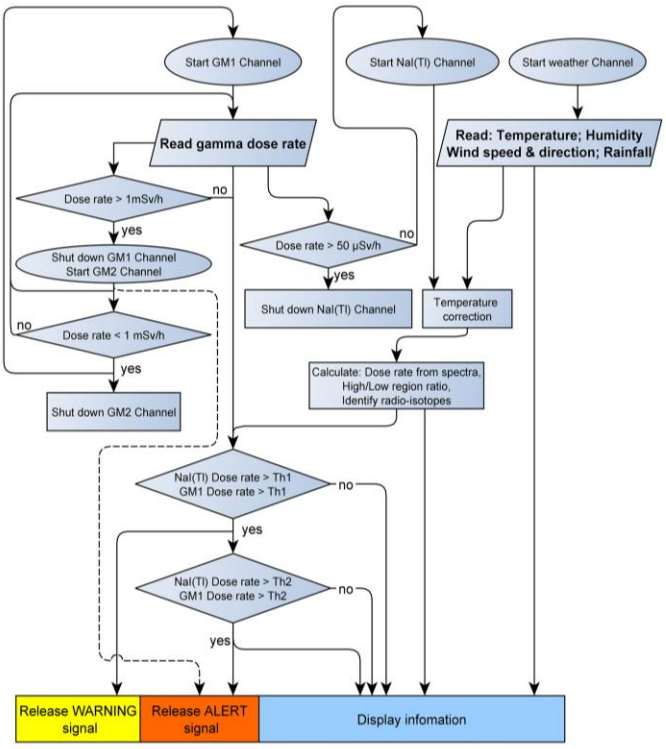

Fig. 3. Flow chart of the control algorithm of the ERMS

1) Data stabilization

The ambient temperature value changes during the day, and the pulse amplitudes of the NaI(Tl) detector is affected by these temperature fluctuations. To remove the influence of temperature from the measured data, the discontinuous gain method is applied to stabilize the gamma spectrum [18]. The measured spectra are adjusted by using a computer program integrated into the central control software. The pulse amplitude is compensated for gain drifts due to the temperature variation. The relationship between the i^{th}-channel position C_{ik} and C_{i0} in a gamma-ray spectrum measured at the arbitrary temperature T_k and reference temperature T_0 (T_0 = 25 ℃ in this study) is described in (1).

$$C_{ik} = C_{i0}.f_i(T_k), \quad (1)$$

where $f_i(T_k)$ is a polynomial function with parameters that have been fitted from experimental data, including the channel positions and peak energy according to the temperature.

2) Dose evaluation

The ambient equivalent dose rates are evaluated in two ways. For the GM channels, the dose rates are calculated by multiple count rates with conversion factors determined directly through calibration in a standard radiation field [19]. The conversion code is embedded into the microcontroller. For the NaI(Tl) channel, the dose rate is based on the spectrum and dose-response of the NaI(Tl) detector; this calculation method is described in [20] and based on the following equation:

$$\dot{D}_{air} = \int_{E_{min}}^{E_{max}} n(E).G(E).dE, \quad (2)$$

where $\dot{D}_{air}$ is the absorbed dose rate in air, E_{min} and E_{max} are the thresholds for deposited energy, E is the energy deposited in the crystal, $n(E)$ is the count rate at energy E in the spectrum, and $G(E)$ is a function determined by unidirectional irradiation geometry. In an actual contaminated environment, the incident direction of the photons depends strongly on source conditions. The above-mentioned $G(E)$ function has the potential to underestimate the air dose rates in the environment by approximately 20% for values of E less than 200 keV and an almost similar amount for higher energy in various irradiation geometries (e.g., radiation from an airborne plume) [20].

Photo-peaks in gamma spectra are determined automatically by a generalized second difference algorithm. This method was proposed originally by Mariscotti [21] and later enhanced by Koskelo [22]. The control program calculates the second difference of the counting rate as a function of photon energies. The peak location, width, height, and intensity are extracted from the gross count without delay by utilizing this algorithm.

To identify artificial radioactivity from accidents involving radioactive materials quickly, the ratio of the count rates in low-

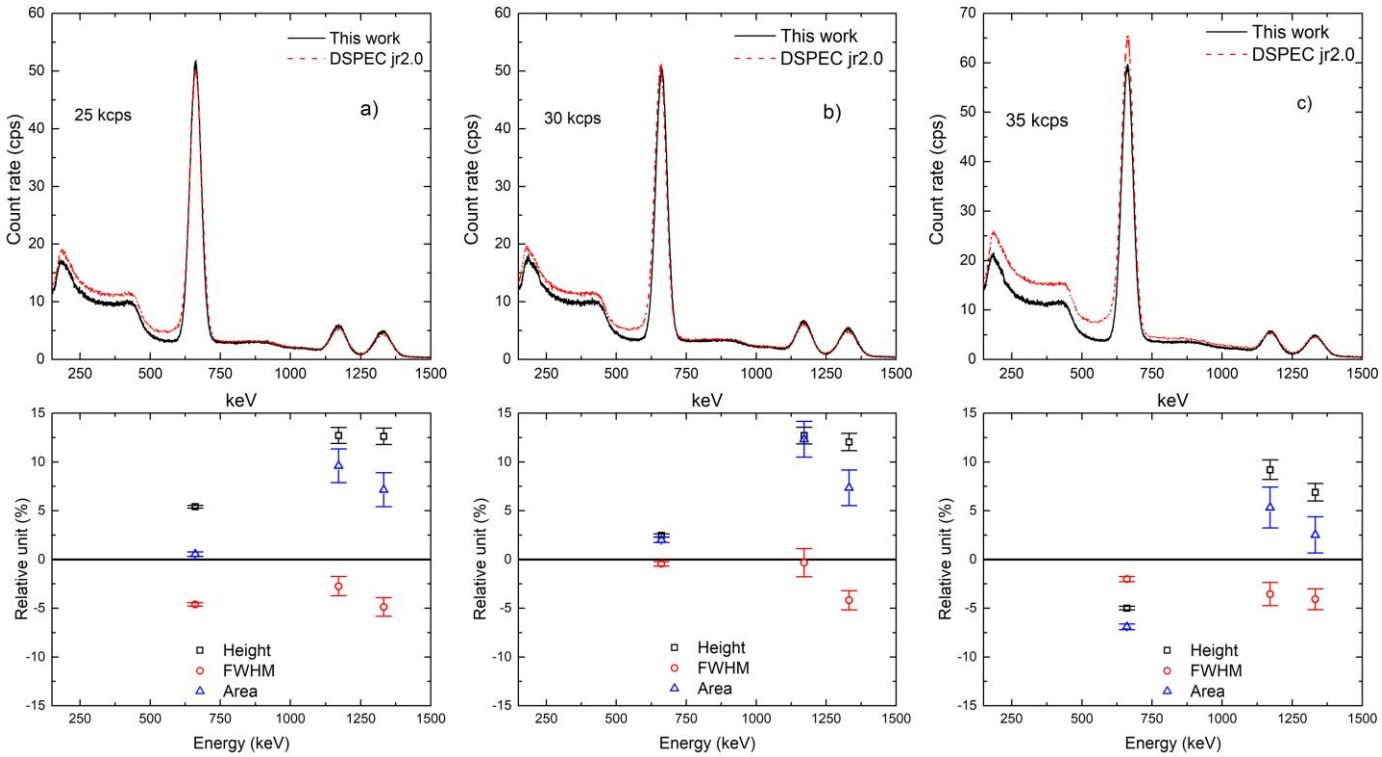

Fig 4. Comparison of the gamma spectra measured with ^{137}Cs and ^{60}Co mixed radioactive sources measured by our DMCA and DSPEC jr 2.0 at 25, 30, and 35 kcps. The upper panels present the gamma spectra normalized to count per second unit. The lower panels reveal the relative differences in FWHM, peak areas, and peak heights according to the spectra presented in the upper panels. The negative relative difference signifies that the value obtained with our DMCA is smaller than that obtained with the DSPEC jr 2.0, whereas the positive relative difference signifies that the opposite has occurred.

energy and high-energy regions of the gamma energy spectrum is calculated. The separation energy point that defines boundary between high-energy and low-energy regions is evaluated through a series of experiments. In the high-energy region, the main components of the naturally occurring radioactive materials (NORMs) are ^{222}Rn daughters, ^{214}Bi, and ^{214}Pb (main peaks are 1120 and 1760 keV, respectively); therefore, the artificial part of the measured radiation is calculated via the ratios for each total gamma counting value over a given period as follows [23]:

$$AP = \sum_{50\ keV}^{E_{Separation}} C_i - CR_{BG} \times \sum_{E_{Separation}}^{3000\ keV} C_i\ , \qquad (3)$$

where AP is the artificial part in the measured spectra, $E_{Separation}$ is the separation energy, C_i is the count rate for channel i, and $CR_{BG} = \frac{\sum_{E=50\ keV}^{E_{Separation}} C_i}{\sum_{E_{Separation}}^{E_{3000\ keV}} C_i}$ is the count rate ratio computed from background spectrum.

3) Confidence improvement

The dose decision threshold is based on ISO 11929:2010 for ionizing radiation measurements and application [24]. The alarm dose threshold confidence interval has a confidence level $k_{1-\alpha}$ = 1.645 and significance level α = 0.05. The computer compares the measured dose rates with the given threshold, and a warning signal is issued when the measured values exceed the first programmed threshold level (Th1).

The gamma spectrometer channel measures gamma-emitting pulses to identify radioisotopes and improve alarm confidence. When a first warning signal appears, the control program checks the measured dose rate. If that value is higher than the second threshold level (Th2), a second warning signal is released. Afterwards, the control program conducts further tests to identify primary exposure sources (i.e., given radioisotopes). The real alarm in the ERMS is turned on only when primary exposure sources are detected in conjunction with the two warning signals. If these warning signals appear but no primary exposure sources are detected, the high-dose-rate warning signal is released, as opposed to turning on the alarm.

III. Evaluation Procedures

A. Evaluation of the DMCA

Several benchmark tests were carried out using a 51×51 mm NaI(Tl) detector (type: 8S8/2.VD.PA.HVG, ScintiTech, USA) and radioactive calibration sources (i.e., ^{137}Cs and ^{60}Co). The performance of our DMCA was compared with that of a commercial DSPEC jr 2.0 at the low count rate (i.e., below 35 kcps). In these assessments, the preamplifier output signal was simultaneously connected to both devices via a signal splitter, namely, MT050 (ORTEC), and the output impedances were kept at 50 Ω to match the two readout devices. The number of gamma-rays attaining by the detector crystal was adjusted by using radioactive sources for different activities as well as changing the source-to-detector distance.

B. Evaluation of the Temperature Stabilization

To evaluate the quality of the temperature stabilization procedure integrated within the ERMS, the measured gamma spectra with and without applying the temperature stabilization procedure in an open environment (i.e., in a real scenario) were

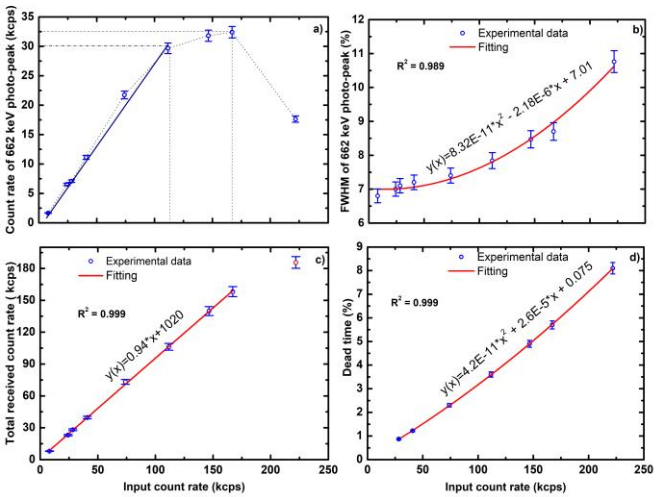

Fig. 5. The FWHM, 662 keV peak count rate, dead time, and total count rate from the ^{137}Cs gamma spectrum as functions of the input count rate.

compared. Measurements were taken for 24 hours. During this time, the temperature fluctuated within the range of 30 ℃ to 42 ℃. This temperature stabilization procedure has been proven to function well in a temperature range from 2 ℃ to 50 ℃ [25], which covers the typical temperature range in Vietnam, i.e., from 5 ℃ to 45 ℃, completely. Therefore, the present evaluation constituted an additional test in a real scenario.

C. Evaluation of the Equivalent Dose Rate

The evaluation of the equivalent dose rate for the ERMS was performed in a secondary standard dosimetry laboratory while using a standard radiation field. The standard dose rates are determined by using a standard ^{137}Cs calibration source, a standard ionization chamber LS01, and a standard reference class dose meter UNIDOS[webline].

IV. Results

Fig. 4 compares the gamma spectra at 25, 30, and 35 kcps, as measured by the DMCA and DSPEC jr 2.0 coupled with the same NaI(Tl) detector. The upper part shows the spectra, whereas the lower part reveals the relative differences between

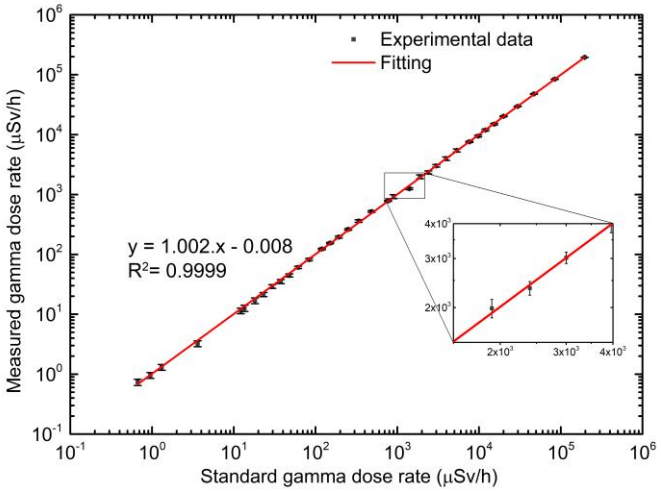

Fig. 6. Ambient equivalent dose rate response for the ERMS with the GM counter; the points represent experiment values measured at the secondary standard dosimetry laboratory.

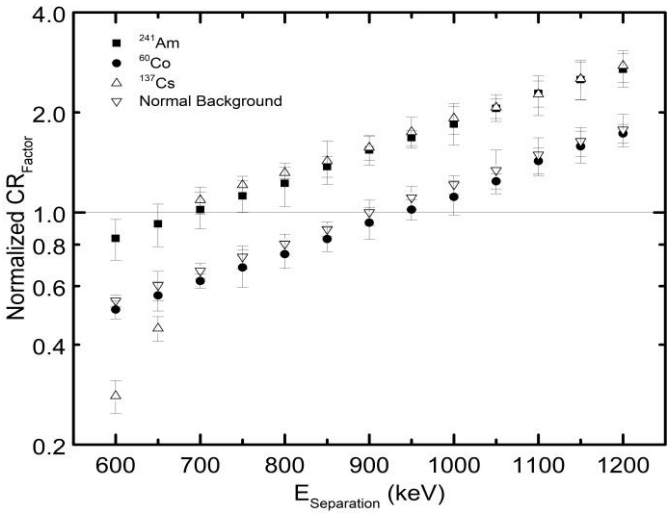

Fig. 7. Distribution tendency for the low/high spectra region ratio to separation energy with the detector; the upper and lower points are calculated by normalized 1 Bq ^{60}Co, ^{137}Cs, and ^{241}Am radiation sources at the surface of detector; The count rates ratio of normal background is normalized to unity at 900 keV.

their peak areas, FWHMs, and peak heights. As can be seen in the upper part, the spectra obtained with the two instruments are slightly different when measured at the three count rates. The analysis results indicate that the FWHM and peak heights obtained from our DMCA are better than those obtained from the DSPEC jr 2.0 up to 12%.

Fig. 5 shows the count rate for the 662 keV peak, the FWHM, the total count rate, and the dead time for the gamma spectrum measured with ^{137}Cs as functions of the input count rate (i.e., the number of gamma rays attained by the detector crystal). Fig. 5c demonstrates the linear correlation between the total count rate and the input count rate for up to 160 kcps. The detector dead-time is seen to effect the total count rate at 220 kcps. The quadratic correlation between the input count rate and the lost count rate is also observed clearly in Fig. 5d. However, the linearity between the peak count rate and the input count rate is valid up to 110 kcps only. Such high input count rates rarely occur in environmental measurements; thus, the linearity of our DMCA satisfies the requirements for any ERMS.

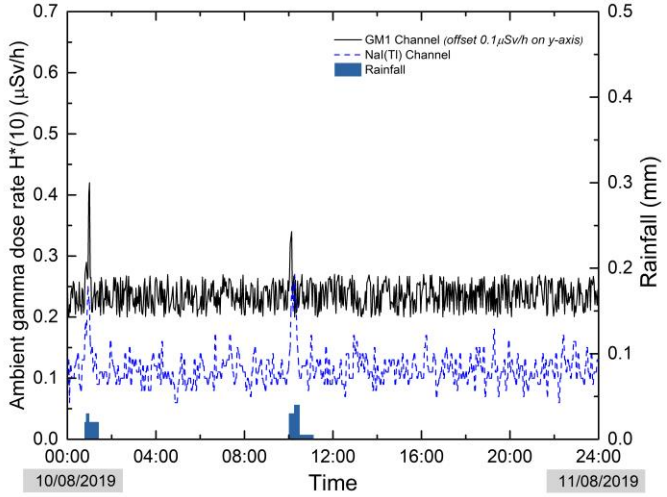

Fig. 8. A typical ERMS dose rate and rainfall data at 5-minute intervals for the NaI(Tl) channel and 2-minutes intervals for the GM1 and weather channels.

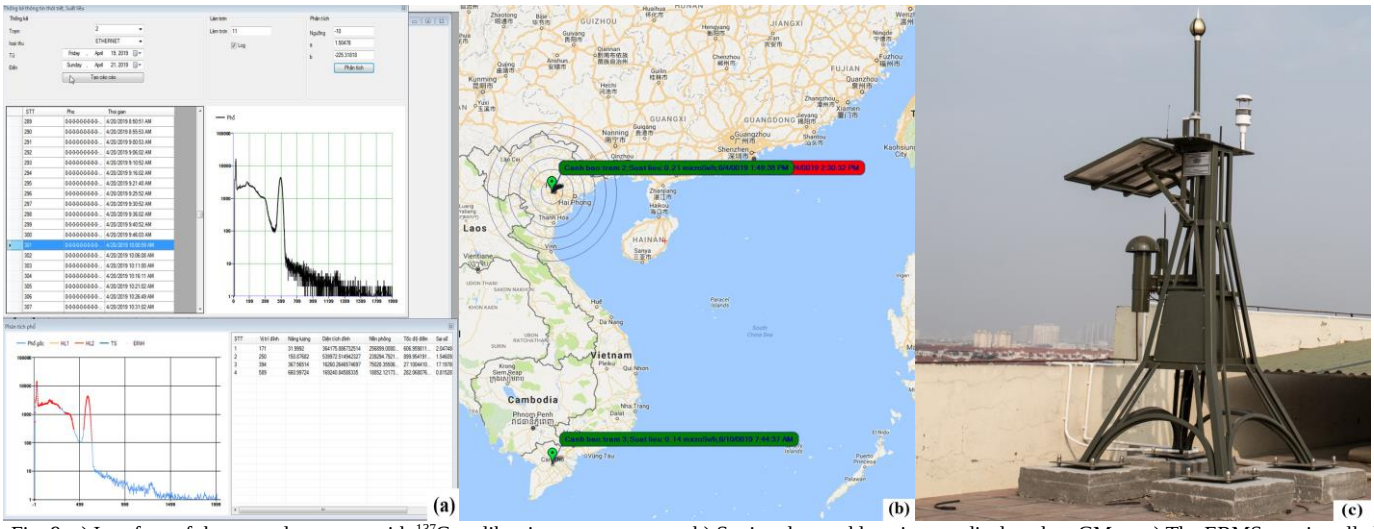

Fig. 9. a) Interface of the control program with ^{137}Cs calibration source spectra; b) Station data and location are displayed on GMap; c) The ERMS was installed on the top of building in Hanoi, Vietnam.

Moreover, the spectra are quite stable when the input count rates below 110 kcps since the energy resolution changes very slightly within this input range (approximately 1%, as clearly shown in Fig. 5b. The gamma dose rate response of the ERMS is presented in Fig. 6, in which the calibration method used by the Institute for Nuclear Science and Technology-VINATOM is described, as in Calibration Procedure RPC.PP-02-15 [19]. With the gamma dose rates ranging from 0.5 μSv/h to 0.2 Sv/h when using the standard radioactive source ^{137}Cs, the accuracy of the measured dose rate is within ±12%. In particular, the standard deviation of the measured gamma dose rate is less than 10%, which is illustrated in the insert figure. Obviously, the dose rate exhibits a linear response for up to 1000 μSv/h.

The $E_{Separation}$ value in (3), the energy with defines the boundary between high and low regions of the gamma energy spectrum was scanned in Fig.7, showing the relationship between the separation energy ($E_{Separation}$) and the count rates ratio in the high and low spectral regions. The chosen level clarifies whether the cause-effect exposure dose belongs to a natural or artificial source. The algorithm for photopeak and radio-isotopes identification works only when the peak region appears clearly on the spectrum (the area of the photopeak should be greater than the standard deviation of the underlying background). This condition is not always satisfied, especially in the presence of a high background level. On the other hand, Compton scattering reduces the total absorption peak efficiency, making it more difficult to identify isotopes via the photopeak detection algorithm. In order to quickly identify the radioactive agent when the environmental background radiation is higher than normal and there are poor statistical peaks, the ratio between spectral regions is utilized. The theoretical basis for this method was developed by C. Wedekind [3]. However, detectors have different efficiencies and Compton scattering regions. Otherwise, the background level for each deployment area would be diverse; hence, it is necessary to carry out experiments to determine the proper separation energy.

After serial testing in the laboratory, the ERMS was installed on the top of a building for operations in a real-life scenario. A typical ERMS exposure rate and rainfall data collected during a 24-hour period are shown in Fig. 8. Fig. 9a and 9b present the interface of the program, while Fig. 9c shows an image of the system. After one year in operation, the ERMS has been operated confidently, delivering relevant measurements and without triggering any false alarm.

V. Discussion

This paper proposed and implemented an ERMS for a case study conducted in Hanoi, located in northern part of Vietnam. The technical design of the system has been presented in detail. Based on the current literature, this type of explanation has seldom been provided. Therefore, this work could partially fill a gap in the literature.

The proposed ERMS combines three channels for radioactive measurements, one channel for monitoring weather parameters, multimodal data transmission methods (cellular network, satellite, ethernet, and RF), and diverse power supplies (a solar panel, a rechargeable battery, and electrical grid). Hence, this system could operate constantly under any conditions. Furthermore, it is more quantitative than the previous systems reported in [2] and [3]. The quantitative information on the radiation field that would be effective in the event of high-level radiation exposure is presented clearly. In Yang Ishigaki et al. [4], data processing is implemented by a smart phone application, and the user can monitor the radiation status in a real-time manner. However, there are many kinds of smart phones with different operating systems, leading to complexities in the development of a compatible program. In our system, a user with a smart or feature phone can also receive alerts from the monitoring system. On the other hand, the evaluation of the temperature stabilization was thoughtfully presented in [24], in which we concluded that our temperature-stabilization component is suitable for implementation on ERMSs with working temperature ranges from 4 ℃ to 45 ℃. We have also pointed out that without the temperature stabilization, the measured gamma spectra are almost impractical (see, e.g., Fig. 7 of [24]). Therefore, the temperature stabilization is an important component of the present ERMS,

particularly since there have been no false alarms up to this point. Its importance will be confirmed in the years to come.

VI. Conclusion

In this study, a configuration of an ERMS with abundant measuring channels and data transmission, high significance, and low cost was successfully implemented. After one year of operation in a real-life scenario with 24-hour monitoring, this prototype still works effectively, reliably, and without any data dropout. Consequently, this EMRS could be installed in a remote border area or on far islands; the system will be of use in generating early warnings of increased radiation levels, along with site-specific meteorological information. In addition, after combining the radiation data with the meteorological parameters, accidents and radionuclide dispersions can be analyzed promptly and precisely.

References

[1] T. Ohba, S. Takimoto, Y. Kitada, T. Tsunoda, A. Kobayashi, and K. Ishida, "Environmetal radation monitoring system development for atmospheric plumes from light water reactor nuclear power plants," *Nucl. Technol.*, 1982, doi: 10.13182/NT82-A32917.

[2] E. Vax *et al.*, "An integrated approach for multi purpose fast deployment environmental radiation monitoring system," in *IEEE Nuclear Science Symposium Conference Record*, 2009, doi: 10.1109/NSSMIC.2009.5401561.

[3] C. Wedekind, G. Schilling, M. Grüttmüller, and K. Becker, "Gamma-radiation monitoring network at sea," *Appl. Radiat. Isot.*, 1999, doi: 10.1016/S0969-8043(98)00062-1.

[4] Y. Ishigaki, Y. Matsumoto, R. Ichimiya, and K. Tanaka, "Development of mobile radiation monitoring system utilizing smartphone and its field tests in Fukushima," *IEEE Sens. J.*, 2013, doi: 10.1109/JSEN.2013.2272734.

[5] James Grichnik, "Radiation monitoring system," US20050242289A1, 2005.

[6] Zhengyi Yang, "Environmental radiation remote early warning monitoring system," CN105589088A, 2016.

[7] ENVINET GmbH, "SARA-80X." Hans-Pinsel-Str. 4, 85540 Haar / Munich, , Germany, 2018.

[8] Dag Stranneby, *Digital Signal Processing*. Jordan Hill: Elsevier Science and Technology Book, 2014.

[9] A. Amara, F. Amiel, and T. Ea, "FPGA vs. ASIC for low power applications," *Microelectronics J.*, 2006, doi: 10.1016/j.mejo.2005.11.003.

[10] VacuTec Meßtechnik GmbH, "VacuTec 70035." Dornblüthstraße 14a, D-01277 Dresden, Germany.

[11] VacuTec Meßtechnik GmbH, "VacuTec 70018A." Dornblüthstraße 14a, D-01277 Dresden, Germany.

[12] V. M. H. Hung Tien Dinh, Chien Kim Dinh, Hiep Van Cao, Anh Huy Phan, "A cost effective quasi-zero dead time digital multi channel analyzer," *J. Mil. Sci. Technol.*, vol. 57A, no. Special Issue, pp. 88–96, 2018.

[13] M. Ouda, M. El_Tokhy, S. Hashima, I. Mahmoud, M. Amal-Eldin, and N. Ziedan, "Hardware Implementation for Pileup Correction Algorithms in Gamma_Ray Spectroscopy," *Int. J. Comput. Appl.*, vol. 176, Jul. 2017.

[14] A. K. George and H. Adjei, "A Design of a low-pass FIR filter using Hamming Window Functions in Matlab," Apr. 2020, doi: 10.7176/ceis/11-2-04.

[15] Glenn G. Knoll, *Radiation Detection and Measurement (4th Edition)*. 2010.

[16] I. I. Mahmoud, M. S. El-Tokhy, and H. A. Konber, "Pileup recovery algorithms for digital gamma ray spectroscopy," *J. Instrum.*, 2012, doi: 10.1088/1748-0221/7/09/P09013.

[17] I. Met One Instruments, "AIO 2 Sonic Weather Sensor." 1600 NW Washington Blvd, Grants Pass, OR 97526, USA.

[18] R. Casanovas, J. J. Morant, and M. Salvadó, "Temperature peak-shift correction methods for NaI(Tl) and $LaBr_3$(Ce) gamma-ray spectrum stabilisation," *Radiat. Meas.*, 2012, doi: 10.1016/j.radmeas.2012.06.001.

[19] Institute for Nuclear Science and Technology, "Dose/Dose rate meters for radiation photon at protection level. The calibration according to $(K_{air})^{\cdot}$, $H^*_{(10)}$, $R^{\cdot}$ quantities with radiation qualities in accordance with ISO 4037 ^{137}Cs, ISO N40, N60, N80 and L70 X-ray beams." 2018.

[20] S. Tsuda and K. Saito, "Spectrum–dose conversion operator of NaI(Tl) and CsI(Tl) scintillation detectors for air dose rate measurement in contaminated environments," *J. Environ. Radioact.*, 2017, doi: 10.1016/j.jenvrad.2016.02.008.

[21] M. A. Mariscotti, "A method for automatic identification of peaks in the presence of background and its application to spectrum analysis," *Nucl. Instruments Methods*, 1967, doi: 10.1016/0029-554X(67)90058-4.

[22] M. J. Koskelo, P. A. Aarnio, and J. T. Routti, "SAMPO80: An accurate gamma spectrum analysis method for minicomputers," *Nucl. Instruments Methods*, 1981, doi: 10.1016/0029-554X(81)90209-3.

[23] A. E. Proctor, "Aerial radiological surveys," doi: 10.2172/6084.

[24] International Organization for Standardization (ISO), "ISO-11929:2010 Determination of the characteristic limits (decision threshold, detection limit and limits of the confidence interval) for measurements of ionizing radiation — Fundamentals and application," *Test*, 2000, doi: 10.5594/J09750.

[25] D. T. Hung *et al.*, "Gamma spetrum stabilization for environmental radiation monitoring stations using NaI(Tl) detector," *Radiat. Prot. Dosimetry*, 2020, doi: 10.1093/rpd/ncaa011.